AIAA JOURNAL
Vol. 46, No. 10, October 2008

Control of Poststall Airfoil Aerodynamics Based on Surface Perturbation

M. M. Zhang,* Y. Zhou,† and L. Cheng‡
Hong Kong Polytechnic University, Hung Hom, Kowloon, Hong Kong

DOI: 10.2514/1.35792

This paper presents an experimental investigation on the control of airfoil aerodynamics at poststall angle of attack α using a surface perturbation technique. Piezoceramic actuators were deployed to create a local surface perturbation on a NACA0012 airfoil, along with an open-loop control system, to manipulate flow around the airfoil. Two different control signals were examined, i.e., square and sine waves. Whereas the lift and drag forces were measured using a load cell, the flow was documented using a particle image velocimetry, laser Doppler anemometer and a single hot wire. The surface perturbation significantly improved the airfoil aerodynamics for $12 \leq \alpha \leq 20$ deg. The control effect with the square-wave excitation was found to be much more effective than that with the sine wave. The control was most effective at $\alpha = 14$ deg: the mean lift coefficient, lift-to-drag ratio, and figure of merit (i.e., the ratio of the power to aerodynamic efficiencies) were enhanced by 35, 64, and 44%, respectively, whereas the mean drag coefficient dropped by 23%. Furthermore, the airfoil stall was postponed by 3 deg. The physics behind the observations were discussed in detail.

I. Introduction

FLOW separation from an airfoil at poststall angle of attack α, due to a large adverse pressure gradient, results in lift decrease, drag increase, and pressure recovery loss [1–3]. This phenomenon frequently occurs in engineering applications such as aircraft, turbomachines, wind turbines, and airfoil-shaped vaned diffusers, which are widely used in centrifugal compressor stages for dynamic pressure recovery, and sets a constraint or limit on the performances of these applications. Naturally, flow manipulation to improve the aerodynamics of airfoils has received a great amount of attention in the literature.

Many control techniques have been developed in the past, which may be classified into two categories, i.e., passive and active controls [4]. The passive control, requiring no external energy input, often relies on reshaping airfoil geometry [5], adding ailerons, flaps, slats, or fences to airfoils [6], and passively transpiring air through the slots on the airfoil surface [7] to postpone flow separation from the airfoil. This kind of technique can only disturb the normal evolution of the flow around the airfoil, instead of flow itself, and thus its performance is rather limited.

In contrast, the active control technique involves an external energy transfer to the flow via actuators to create a desirable effect on flow separation and, subsequently, on the airfoil aerodynamics. For example, Seifert et al. [8] introduced an oscillatory blowing from the surface of an NACA0015 airfoil to disturb the flow around the airfoil, and effectively postponed flow separation from the airfoil from $\alpha = 12$ to 14 deg. As a result, the mean lift coefficient $\bar{C}_L$ was increased by 68%, whereas the mean drag coefficient $\bar{C}_D$ dropped by 32%. Sinha [9] embedded a capacitively actuated flexible membrane transducer near the leading edge of a NACA0012 airfoil to control flow separation from the airfoil. This actuator had a potential to modulate the local pressure gradient of the airfoil near the actuation area and, subsequently, flow separation from airfoil, which was ascribed to an amplified transmissive perturbation by the actuator within the airfoil boundary layer. Zaman et al. [10] and Hsiao et al. [11] installed a loudspeaker outside an LRN(1)-1007 airfoil and inside a NACA 63_3-018 airfoil, respectively. The acoustic excitation from the loudspeaker suppressed flow separation. In both cases, there was a maximum increase of 50% in $\bar{C}_L$ at $\alpha \geq 18$ deg. Although these traditional active techniques are effective, the aerodynamic gains made by them are often offset by their inherent drawbacks, such as too many auxiliary equipments, excessive weight, and high excitation level.

In the past decade, smart-material-based technology has become the enabler that cuts across traditional boundaries between material science and engineering. One of the typical products produced out of this smart technology is the advanced piezoceramic actuator, which is often smaller, lighter, and more energy-efficient than many traditional actuators. This type of actuator has been used to develop new active flow-control techniques. Seifert et al. [12] mounted an array of piezoceramic actuators along the span of a PR8-40-SE (Israel Aircraft Industries) airfoil. Once excited, these actuators could oscillate in-phase or antiphase to each other, creating a favorable effect on flow separation from the airfoil and achieving an increase in $\bar{C}_L$ up to 22% and a decrease in $\bar{C}_D$ up to 20%, compared with the uncontrolled flow, for $\alpha = 8 \sim 18$ deg. Melton et al. [13] placed a piezoceramic actuator at the leading edge of a NASA energy-efficient transport high-lift airfoil to manipulate the flow and successfully postponed the flow separation, achieving a maximum increase in $\bar{C}_L$ by 15% at $\alpha = 15$ deg. Cheng et al. [14] recently developed a surface perturbation technique, based on piezoceramic actuators, to manipulate a square-cylinder wake, which proved to be very effective in manipulating, either enhancing or suppressing, vortex shedding from the cylinder [15,16]. Both open-loop and closed-loop control were deployed. One naturally wonders whether this surface perturbation technique, combined with the control approach, could be applied to control flow separation from an airfoil. Flow separation from a cylinder is characterized by flip-flop alternate vortex shedding from the two sides of the cylinder. On the other hand, the roll up of the shear layer over the suction side of the airfoil does not seem to interact so vigorously with vortices generated at the trailing edge. This difference implies that a flow-control technique that is effective in the manipulation of flow separation from a cylinder may not work well for that from an airfoil.

In this work, we investigate how to adapt the surface perturbation technique, based on ceramic actuators, to the effective control of flow separation from a NACA0012 airfoil. Different activating signals

Received 21 November 2007; revision received 20 March 2008; accepted for publication 6 April 2008.

*Department of Mechanical Engineering; currently Mechanical Engineering Department, Johns Hopkins University, 223 Latrobe Hall, 3400 North Charles Street, Baltimore, Maryland 21218; mingming@jhu.edu.

†Corresponding Author, Department of Mechanical Engineering; mmyzhou@polyu.edu.hk.

‡Department of Mechanical Engineering.

were examined, including square- and sine-wave signals. The control performance was evaluated in terms of the forces on the airfoil, which were measured using a load cell. To understand the underlying physics, the control effect on the flowfield around the airfoil was measured and analyzed in detail using a particle image velocimetry (PIV), a laser Doppler anemometry (LDA), and a single hot wire.

II. Experimental Details

Experiments were carried out in a closed-circuit wind tunnel with a square working section (0.6 × 0.6 m) of 2.4 m in length. The wind speed was adjusted with a frequency inverter and measured with a Furness electronic micromanometer (FCO510), whose experimental uncertainty was estimated to be about 2%. The designed wind-speed range in the working section is 2–50 m/s, over which the flow has been confirmed to be stable. For example, the flow nonuniformity is 0.2% and its longitudinal turbulence intensity is 0.1% at 2.4 m/s. Readers may refer to Huang et al. [17] for more details about the tunnel. A NACA0012 airfoil with a chord length of $c = 250$ mm and a span length of $l = 550$ mm was horizontally fixed on both sides of the test section through a pitching pivot (Fig. 1a). For simplicity, measurements were only conducted at a typical freestream velocity $U_\infty = 3$ m/s, corresponding to the Reynolds number Re_c ($U_\infty c/\nu$,

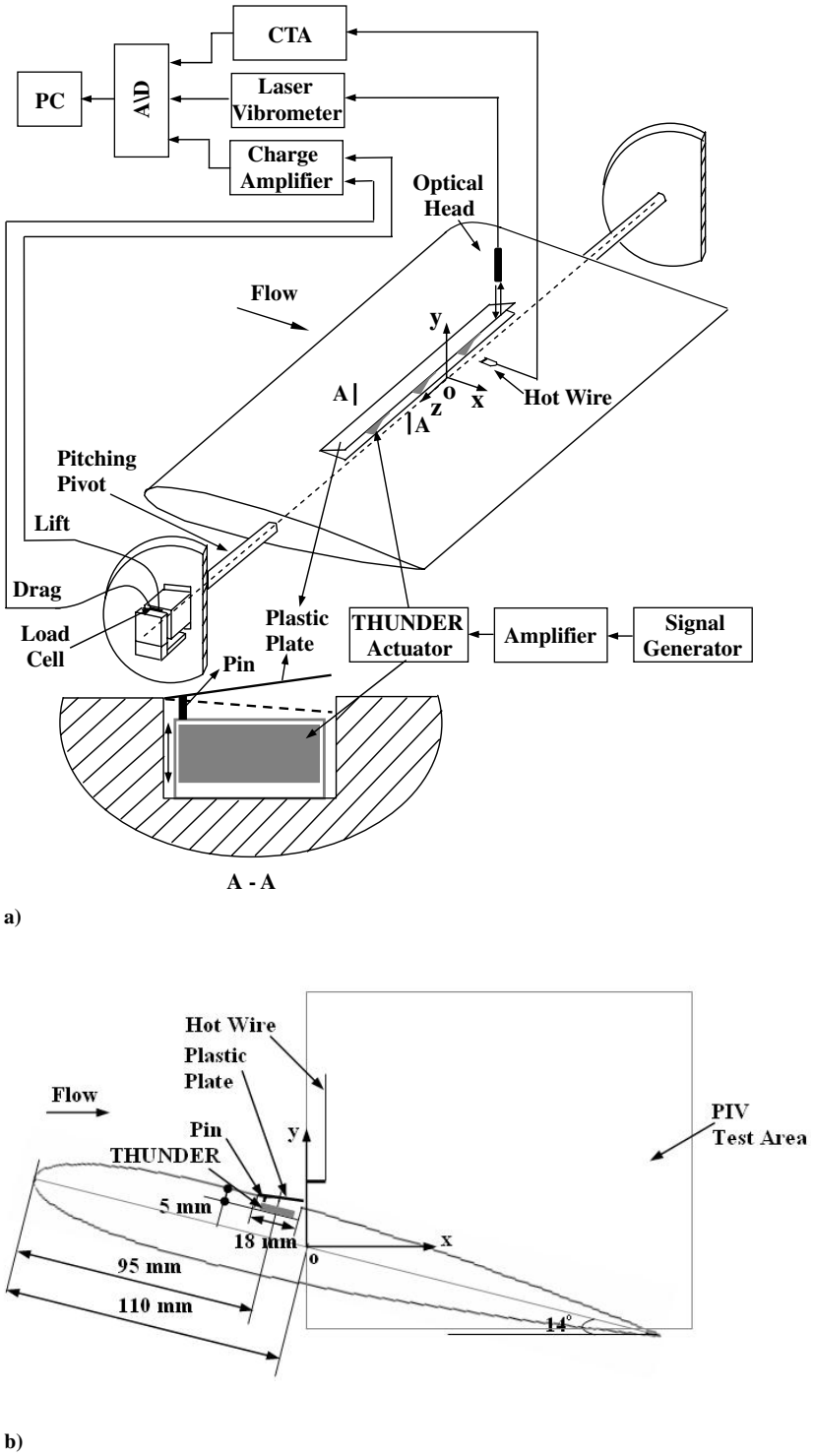

Fig. 1 Airfoil a) experimental arrangement, and b) cross section ($\alpha = 14$ deg), the location and dimension of the control mechanism, the hot-wire position, and the PIV measurement area.

where ν is the kinematic viscosity) of 4.9×10^4, to demonstrate the control effect. At this Re_c and poststall α, the flow over the airfoil has already transited to turbulence [18].

Three curved piezoceramic THUNDER actuators (thin layer composite unimorph piezoelectric driver and sensor) were embedded inside a slot 290 mm long, 18 mm wide, and 5 mm deep on the upper side of the airfoil, which was 95 mm or $0.38c$ from the airfoil leading edge, shown in Fig. 1b. Seifert et al. [12] used similar piezoceramic actuators to the present ones, though much larger in size, to enable effective actuation, and demonstrated an effective improvement in airfoil aerodynamics when the actuators were placed near $0.4c$ from the airfoil leading edge. Note that, because the actuation spans only 53% of the whole airfoil, the actuation could produce a three-dimensional effect on the flow, which is unlikely to be significant because of the small oscillation amplitude (a maximum root mean square value of 1.8 mm) of the actuators. The THUNDER actuators, developed by the NASA Langley Research Center and produced by FACE International Corp., deform out of plane under an excitation voltage. THUNDERs have many advantages over conventional piezoceramic actuators, such as large displacement, acceptable load capacity, and small size. Typically, without any loading, the present actuator (THUNDER-8R) with a physical dimension of $63 \times 14 \times 0.43$ mm may oscillate at a maximum displacement of about 2 mm (without any loading) and a frequency of up to 2 kHz [19]. The actuators were cantilever-installed to create the maximum perturbation displacement in a direction approximately normal to the airfoil surface and thus the best control performance under the same excitation condition [15]. The actuators and the walls of the slot around the actuators were well lubricated to minimize the contact friction. A plastic plate covered the slot, flush with the airfoil surface. One side of the plate near the front corner of the slot was fixed and the other side was free to form a "flap" (see the cutout in Fig. 1a). The plate was connected with the three actuators separately using three small pins. Driven by the actuators, the plate would oscillate to create a local perturbation on the flow. The actuators were simultaneously activated by a signal with controllable frequency f_p, voltage V_p, and waveform, generated by a signal generator (model DS345) and amplified by two dual-channel piezodriver amplifiers (Trek PZD 700). The natural frequency of these installed actuators was about 8 Hz, at which the root mean square value of the perturbation displacement $Y_{p,\mathrm{rms}}$ ($V_{p,\mathrm{rms}} = 141$ V) was largest, up to about 1.8 mm (Fig. 2a). In addition, at $f_p = 8$ Hz, $Y_{p,\mathrm{rms}}$ increased with the increasing rms value of V_p, i.e., $V_{p,\mathrm{rms}}$ (Fig. 2b), though not linearly [20].

The mean lift and drag forces L and D were measured using a three-component load cell (Kistler 9251A) mounted at one end of the pivot (Fig. 1a). The force-measuring range and sensitivity of the load cell were up to 5 kN and 8 pC/N, respectively. The origin of the coordinate system was defined at the pivot center, with the coordinates x, y, and z along the streamwise, transverse, and spanwise directions, respectively. The distance between the pivot center and the airfoil leading edge along the chord is 110 mm (Fig. 1a). A single hot wire, made of 5 μm tungsten wire, was placed downstream of the perturbation surface at $0 < x/c < 0.008$, $0.1 < y/c < 0.15$, $z/c = 0$ to monitor a possible modification in streamwise fluctuating flow velocity u under control. A dual-beam laser vibrometer (Polytec Series 3000) was deployed to measure the displacement Y_p near the tip of the perturbation surface, i.e., $x/c = -0.02$, $y/c = 0.056$, and $z/c = 0$. This measurement position was determined by moving the laser head to locate the maximum displacement for each excitation frequency f_p and voltage V_p. The measurement uncertainty of the laser vibrometer was about 0.5%. All the measured signals, L, D, u, and Y_p, were conditioned and digitized using a 12-bit a/d board at a sampling frequency of 2 kHz per channel. The duration of each record was about 20 s. In addition, the control effect on the crossflow distributions of the mean flow velocity $\bar{U}$ and $\bar{V}$, and the rms values of the fluctuating velocities u_{rms} and v_{rms}, in the x and y directions, were measured using a two-component LDA system (Dantec 58N40). The measuring volume has a minor axis of 1.18 mm and a major axis of 2.48 mm. The

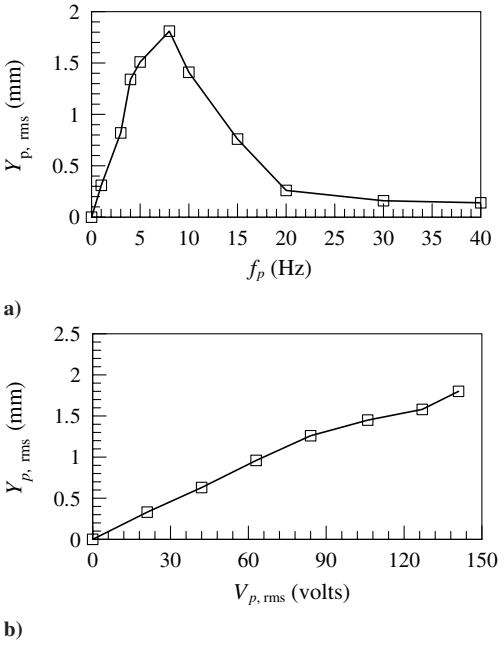

Fig. 2 Effect of control parameters on the perturbation displacement at the tip of the plastic plate when the square excitation was used: a) perturbation frequency, b) perturbation voltage; $\alpha = 14$ deg.

measured mean velocity was estimated to have an error of less than 3% and the corresponding error for measured rms values was less than 10% [21].

A Dantec standard PIV2100 system was used to measure the flow, near the airfoil, in the x-y plane and the y-z plane. Flow was seeded by smoke generated from paraffin oil and was illuminated by two New Wave standard pulsed laser sources of a wavelength of 532 nm, each having a maximum energy output of 120 mJ. Digital particle images were taken using one charge-coupled device camera (HiSense type 13, gain $\times$ 4, double frames, 1280×1024 pixels). A Dantec FlowMap Processor (PIV2100 type) was used to synchronize image-taking and illumination. A wide-angle lens was used so that each image covered an area of 155×135 mm, i.e., $x/c \approx 0 \sim 0.62$ and $y/c \approx -0.12 \sim 0.42$, for the measurement in the x-y plane and 110×60 mm, i.e., $z/c \approx -0.22 \sim 0.22$ and $y/c \approx 0.06 \sim 0.3$, for the measurement in the y-z plane. The image magnifications in the x-y and the y-z plane were 0.12 mm/pixel and 0.08 mm/pixel, respectively. In the image processing, 32×32 rectangular interrogation areas were used. Each interrogation area included 32 pixels with a 25% overlap with other areas. The ensuing in-plane velocity vector field consisted of 53×42 vectors. The spanwise and streamwise vorticity components ω_z and ω_x were approximately derived, based on a central difference scheme, from PIV-measured velocities. The spatial resolution of the vorticity estimate depends on grid spacing, about 2.8 and 1.7 mm, respectively. See Zhang et al. [21] for more details about the PIV measurement.

III. Optimization of Control Performances

A series of tests were performed to determine the optimal parameters of the signal activating the actuators, i.e., the perturbation frequency f_p and the perturbation voltage V_p, under which the mean lift coefficient $\bar{C}_L = L/(0.5\rho U_\infty^2 cl)$ and the mean drag coefficient $\bar{C}_D = D/(0.5\rho U_\infty^2 cl)$ can be effectively enhanced or impaired, where ρ is air density. In view of the presently relatively high-blockage ratio ($\approx$10%), both $\bar{C}_L$ and $\bar{C}_D$ were corrected using an equation proposed by Maskell [22]:

$$\frac{C_1}{C_2} = 1 + \varepsilon \frac{C_1 S_1}{S_2} \tag{1}$$

where C_1, C_2, S_1, S_2, and ε represent the measured coefficient, corrected coefficient, effective blockage area induced by the airfoil,

cross-sectional area of the wind tunnel, and blockage factor (≈0.96), respectively.

Figure 3 shows the results of optimizing f_p and V_p ($\alpha = 14$ deg) under the excitation of a square-wave signal. As step 1, the fundamental frequency f_p was adjusted from 0 to 40 Hz with $V_{p,\mathrm{rms}}$ fixed at the maximum permissible voltage of the actuator (≈141 V) (Fig. 3a). The unperturbed $\bar{C}_L$ and $\bar{C}_D$, as indicated by two dashed lines, are given in the figure to provide a benchmark. At $f_p = 8$ Hz, $\bar{C}_L$ and $\bar{C}_D$ reach the maximum and the minimum, respectively. This is reasonable because the natural frequency of the actuator was presently designed at 8 Hz (Fig. 2). A larger $Y_{p,\mathrm{rms}}$ corresponds to a better performance in controlling fluid–structure interaction [14]. Therefore, the correspondence between the largest $Y_{p,\mathrm{rms}}$ and the best control performance at $f_p = 8$ Hz, i.e., a normalized reduced forcing frequency $F^+(=f_p c/U_\infty)^4$ of 0.67, is not unexpected. One remark is due. The same $Y_{p,\mathrm{rms}}$ should really be applied for the purpose of quantifying the effect of f_p on $\bar{C}_L$ and $\bar{C}_D$. This would be almost impossible because $Y_{p,\mathrm{rms}}$ varies greatly with f_p (Fig. 2a). In step 2, $V_{p,\mathrm{rms}}$ was varied from 0 to 141 V at $f_p = 8$ Hz (Fig. 3b). $\bar{C}_L$ increases monotonically with increasing $V_{p,\mathrm{rms}}$, whereas $\bar{C}_D$ decreases. In step 3, with $V_{p,\mathrm{rms}}$ set at 141 V, f_p was retuned, yielding a very similar result to that in Fig. 3a, with $\bar{C}_L$ and $\bar{C}_D$ reaching the maximum and the minimum, respectively, at $f_p = 8$ Hz. This implies that the optimization of the parameters were already converged in the first three iterations, that is, $f_p = 8$ Hz and $V_{p,\mathrm{rms}} =$ 141 V were the optimal parameters for the square-wave excitation. Note that thus determined optimal control parameters (f_p and V_p), due to a possible inherent coupling between them, might not in general be the best. However, the control performance is presently improved monotonically with increasing $V_{p,\mathrm{rms}}$ (Fig. 3b). With the initial $V_{p,\mathrm{rms}}$ set at the maximum available, the best control performance could be achieved with tuning only f_p. Indeed, after setting $f_p = 8$ Hz, the control performance is not improved any further with changing $V_{p,\mathrm{rms}}$ from 0 to 141 V. Therefore, it is safe to say that the best control performance has been approximately achieved with $f_p = 8$ Hz and $V_{p,\mathrm{rms}} = 141$ V. Figure 4 shows the typical transient behaviors of lift and drag signals when the perturbation, with the optimal parameters used, is applied. It is evident that, under the perturbation, the lift is increased rather remarkably, whereas the drag is effectively reduced.

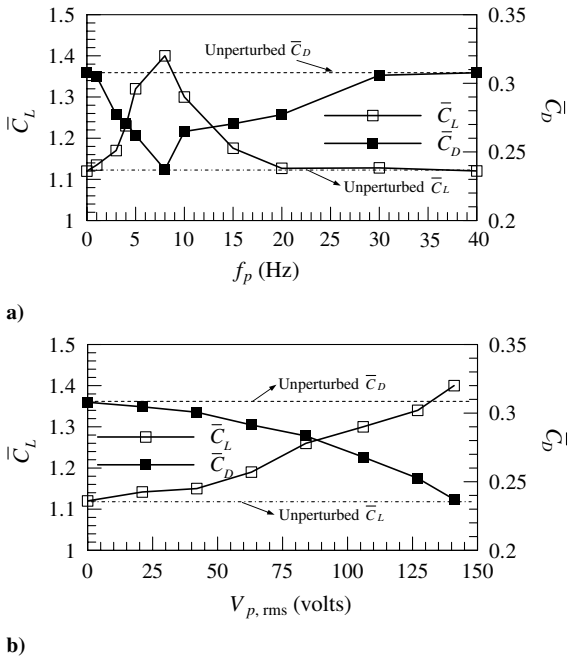

Fig. 3 Effect of control parameters on the mean lift coefficient and drag coefficient when the square wave excitation was used: a) perturbation frequency, b) perturbation voltage; $\alpha = 14$ deg.

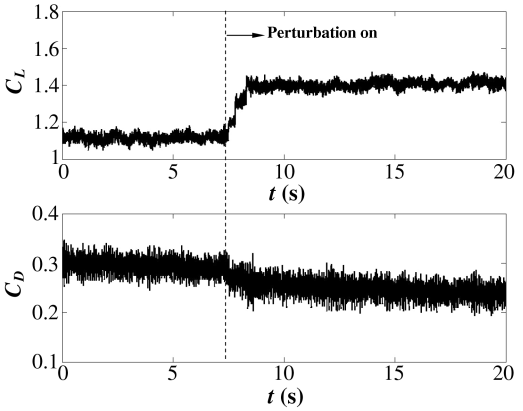

Fig. 4 Typical transition of aerodynamic coefficient signal with and without perturbation when the square wave excitation was used: a) lift coefficient signal, b) drag coefficient signal; $\alpha = 14$ deg, $f_p = 8$ Hz.

The excitation of a sine-wave signal was also examined, following the aforementioned optimization procedure. The results are not shown here. It turned out that, for $\alpha = 12 \sim 20$ deg, $f_p = 8$ Hz and $V_{p,\mathrm{rms}} = 141$ were found to be the optimum parameters, irrespective of the sine- or square-wave excitation. Unless otherwise stated, the results associated with the two optimal parameters will be presented and discussed hereinafter.

IV. Control Performances

The control performance was first evaluated in terms of enhancing $\bar{C}_L$. Figure 5 shows the control effect on $\bar{C}_L$ as α varies from 8 to 23 deg. Both sine- and square-wave excitations were examined. Without control, $\bar{C}_L$ achieves the maximum at $\alpha = 11$ deg, and then declines rapidly. It is well known that, for a NACA0012 airfoil, the stall occurs normally at $\alpha \approx 11$ deg, where the flow begins to separate from the airfoil [23,24]. With the sine-wave excitation introduced, $\bar{C}_L$ increases appreciably at $\alpha > 11$ deg. However, under the square-wave excitation, $\bar{C}_L$ is significantly enhanced for $12 \leq \alpha \leq 20$ deg. The stall angle is increased from 11 to 14 deg and the maximum $\bar{C}_L$ at $\alpha = 14$ deg climbs by 35% compared with the unperturbed case.

The control performance was then evaluated in terms of $\bar{C}_D$, lift-to-drag ratio L/D, and figure of merit (F.M.), which is defined as the ratio of the power to aerodynamic efficiencies:

$$\text{F.M.} = \frac{\eta}{\bar{C}_L/\bar{C}_D} \tag{2}$$

where η stands for the airfoil power coefficient $[\bar{C}_L/(\bar{C}_D + C_E)]$. The input power coefficient C_E is given by $W_i/(0.5\rho l c U_\infty^3)$, where

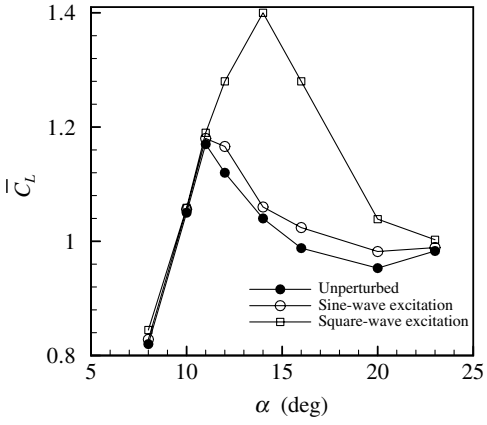

Fig. 5 Mean lift coefficient $\bar{C}_L$ vs angle of attack α with and without perturbation.

Table 1 Comparisons in performances between sine- and square-wave excitations

Excitation	Sine wave				Square wave			
	$\bar{C}_L$	$\bar{C}_D$	L/D	F.M.	$\bar{C}_L$	$\bar{C}_D$	L/D	F.M.
12 deg	4% ↑	6% ↓	13% ↑	11% ↑	13% ↑	18% ↓	46% ↑	23% ↑
14 deg	2% ↑	8% ↓	11% ↑	9% ↑	35% ↑	23% ↓	64% ↑	44% ↑
16 deg	4% ↑	3% ↓	7% ↑	6% ↑	30% ↑	15% ↓	52% ↑	30% ↑
20 deg	3% ↑	2% ↓	5% ↑	4% ↑	9% ↑	9% ↓	20% ↑	14% ↑

W_i is the power applied to the actuators. The figure of merit may be used as a criterion for assessing the power efficiency of a control technique [12]. Table 1 presents $\bar{C}_L$, $\bar{C}_D$, L/D, and F.M. under sine- and square-wave excitations. In both cases, $\bar{C}_L$, L/D, and F.M. are enhanced and $\bar{C}_D$ is reduced, demonstrating not only the effective control of airfoil aerodynamics but also a high-power efficiency of the technique applied. The best control performance was achieved at $\alpha = 14$ deg with the square-wave excitation used; $\bar{C}_L$, L/D, and F.M. climbed by 35, 64, and 44%, respectively, and $\bar{C}_D$ dropped by 23%, compared with the unperturbed flow. It is interesting to note that the square-wave excitation outperforms the sine-wave excitation in every category, resulting in a much higher increase in $\bar{C}_L$, L/D, and F.M., and a more pronounced reduction in $\bar{C}_D$. One explanation is that the square-wave perturbation signal includes not only the fine-tuned fundamental frequency component but also its harmonics (Fig. 6a), which may capitalize optimally the inherent instabilities in the shear layer around the airfoil. On the other hand, the sine-wave one contains only the perturbation-frequency component (Fig. 6a), which might not be able to cover all the inherent instabilities in the shear layer. Margalit et al. [25], Amitay et al. [26], and Bons et al. [27] also observed that the square-wave modulated excitation was superior to the sine-wave excitation when using different kinds of zero-net-mass-flux actuators to control shear layer separation from a Delta airfoil, a unconventional NACA airfoil with a half-circular cylinder as the leading edge and an airfoil-shaped vane, respectively. They also attributed the difference to additional harmonic components in the square wave, and explained that these harmonic components in the square wave might enable a more effective amplification of the most unstable modes of separated shear layer and, subsequently, enhance momentum transfer across the layer. Furthermore, the "effective" control energy associated with the square wave may be greater than that associated with the sine wave. One way to quantify the energy of Y_p ($E_{Y_p,\Delta f}$) associated with the nth harmonic $f_p^{(n)}$ of f_p(=8 Hz) is to integrate E_{Y_p} over a −3 dB bandwidth about $f_p^{(n)}$, which is then multiplied by $Y_{p,\mathrm{rms}}$. The calculated $E_{Y_p,\Delta f}$ with $n = 1, 2, 3, \ldots, 8$ is given in Fig. 6b.

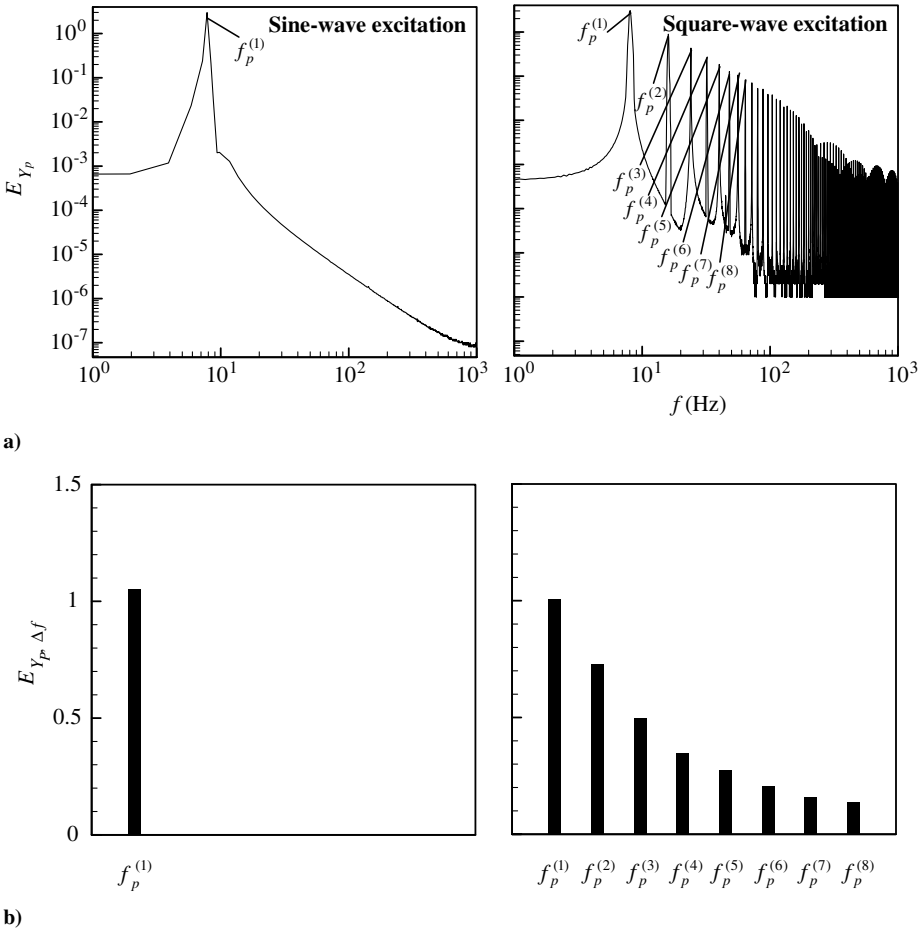

Fig. 6 Comparisons between sine-wave and square-wave excitation in terms of a) the power spectrum of the perturbation displacement signal E_{Y_p}; b) the energy of the perturbation displacement $E_{Y_p,\Delta f}$ corresponding to the main nth harmonics of the fundamental perturbation frequency $f_p^{(n)}$ ($n = 1, 2, 3, \ldots, 8$). $f_p^{(1)} = 8$ Hz, $V_{p,\mathrm{rms}} = 141$ V, $\alpha = 14$ deg.

Apparently, due to the harmonic components, the total of $E_{Y_p,\Delta f}$ under the square-wave excitation is much larger than that under the sine wave, which may be partially responsible for the better performances of the former than the latter. It is worth mentioning that the sine-wave excitation has been widely applied previously [11–13]. The present observation suggests that the control performance of the previous investigations, at least some of them, could have been further improved if a square-wave excitation had been used.

V. Discussions

To gain a better understanding of the underlying control mechanism, the perturbation effect on the flowfield near the airfoil is investigated. All measurements were conducted at $\alpha = 14$ deg, where the control performance is most pronounced (Sec. IV). Figure 7 presents the typical transient behavior of the instantaneous streamwise flow velocity U, as measured using a hot wire placed at $x/c = 0$ and $y/c = 0.1$, when the perturbation was off and on. Although the sine-wave excitation slightly changed U (Fig. 7a), the square-wave excitation increased both the mean and fluctuating components of U (Fig. 7b). The control effect on the global flowfield is reflected in the crossflow distributions of the mean and rms values of the flow velocity in x and y directions, i.e., $\bar{U}^*$, $\bar{V}^*$, u^*_{rms}, and v^*_{rms} (Fig. 8), measured using LDA at $x/c = 0.008$ above the airfoil with and without the perturbation. In this paper, the asterisk denotes normalization by U_∞. The maximum $\bar{U}^*$, $\bar{V}^*$, u^*_{rms}, and v^*_{rms} for $y/c < 0.2$ increases by 7.2, 2.3, 11.5, and 8.0%, respectively, with the sine-wave excitation. The corresponding increase is 34, 13, 36, and 32% with the square-wave excitation. Dandois et al. [28] deployed a zero-net-mass-flux actuator to control flow separation from a ramp, and set the forcing frequency near the frequency of the separated shear layer. They also observed the enhanced mean and fluctuating streamwise velocities. Under the square-wave excitation, the increase in these quantities is discernible at $x/c = 0.128$ (Fig. 9), and even at $x/c = 0.248$ (Fig. 10), though the y/c range, where this increase is appreciable, shrinks. Note the appreciable increase in $\bar{U}^*$ and $\bar{V}^*$ measured at the location ($y/c \approx 0.06$) nearest to the airfoil surface, which is in the boundary layer of the airfoil [1], under the square-wave excitation (Figs. 8a–8d, 9a–9d, and 10a), implying an enhanced momentum in the boundary layer of the airfoil. Note that the increases in u^*_{rms} and v^*_{rms} are not always desirable, which are associated with larger fluctuating lift and drag forces and hence a possible airfoil oscillation to some degree [29,30].

The increased flow velocities due to the perturbation is linked to the generation of large-scale vortices above the airfoil surface [4,31]. Figures 11 and 12 present the typical isocontours of the PIV-measured instantaneous spanwise and streamwise vorticity, i.e., $\omega^*_z = \omega_z c/U_\infty$ and $\omega^*_x = \omega_x c/U_\infty$ at $x/c = 0.008$, with and without perturbation. In the absence of perturbation, flow separation from the airfoil leading edge is evident, forming a rather large recirculation region (Figs. 11a and 12a). However, in the presence of perturbation,

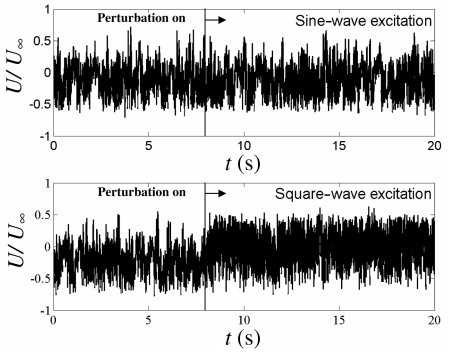

Fig. 7 Typical transition of the instantaneous streamwise flow velocity U when the perturbation was off and on: a) sine-wave excitation; b) square-wave excitation. $\alpha = 14$ deg. The hot wire was located at $x/c = 0$ and $y/c = 0.1$.

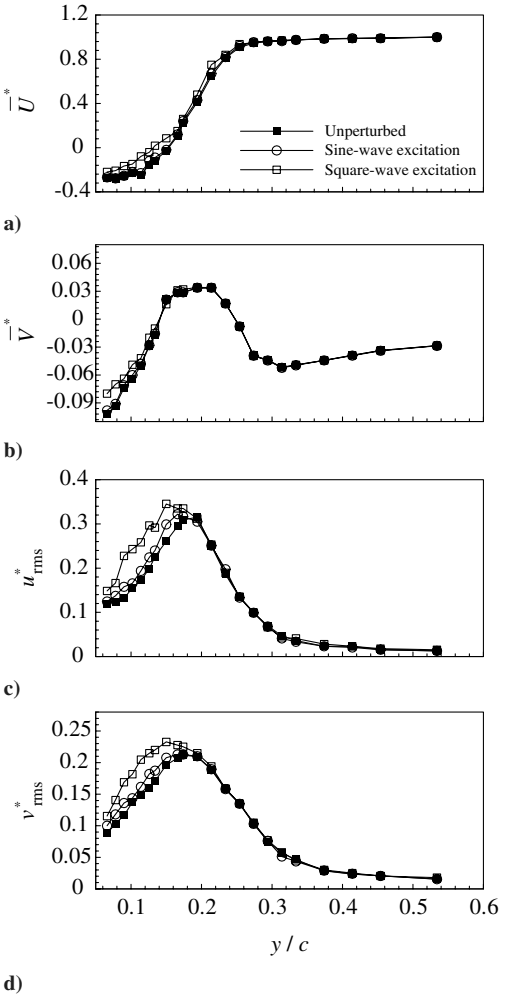

Fig. 8 Crossflow distributions of mean flow velocities and root mean square value of fluctuating flow velocities in the x and y directions at $x/c = 0.008$ with and without perturbation: a) $\bar{U}^*$, b) $\bar{V}^*$, c) u^*_{rms}, d) v^*_{rms}. $\alpha = 14$ deg.

the separated shear layer tends to reattach to the airfoil surface, suggesting a weakened flow separation, which is associated with the generation of vortical structures near the airfoil surface (Figs. 11b, 11c, 12b, and 12c). This is more evident when the square-wave excitation is deployed (Figs. 11c and 12c), where large-scale vortices occur and, accordingly, the recirculation region is minimum. The averaged vortex circulation $\bar{\Gamma}$, estimated based on 45 PIV images in the x-y plane, was enhanced by 39% compared with the uncontrolled case. Each circulation Γ associated with a vortex is estimated by numerical integration [32]

$$\Gamma^* = \frac{\Gamma}{U_\infty c} = \sum_{i=1}^{53}\sum_{j=1}^{42}(\omega^*_z)_{ij}\frac{\Delta A}{c^2}$$

where $(\omega^*_z)_{ij}$ is spanwise vorticity over area $\Delta A = \Delta x \Delta y$, Δx and Δy being the integral step along the x and y directions, respectively. The cutoff level was set at $|\omega^*_{zc}| = 3$, about 6% of $|\omega^*_{z\max}|$, which is similar to that used by Cantwell and Coles [32].

Using numerical simulation and a periodic blowing-suction technique, Wu et al. [24] also made similar observations to that in Fig. 11c on a NACA0012 airfoil for $20 \le \alpha \le 30$ deg when the excitation frequency was equal to the frequency f_s of vortices shed from the airfoil leading edge. They attributed the observation to the lock-in or resonant relationship between flow and excitation. Under the resonant condition, the unfavorable random modes that exist in the unperturbed flow would be suppressed, making the unstable dominating vortex mode more periodical and stronger. This

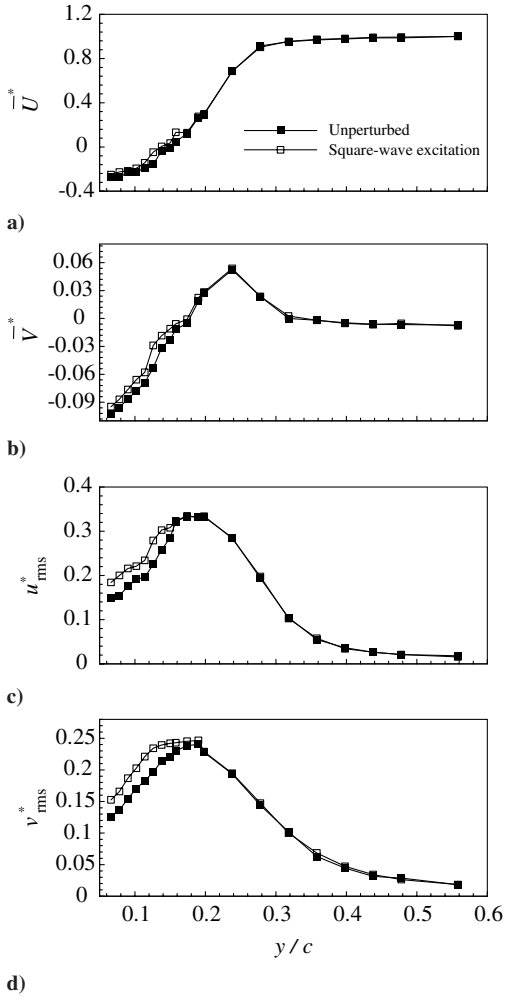

Fig. 9 Crossflow distributions of mean flow velocities and root mean square value of fluctuating flow velocities in the x and y directions at $x/c = 0.128$ with and without perturbation: a) $\bar{U}^*$, b) $\bar{V}^*$, c) u^*_{rms}, d) v^*_{rms}. $\alpha = 14$ deg.

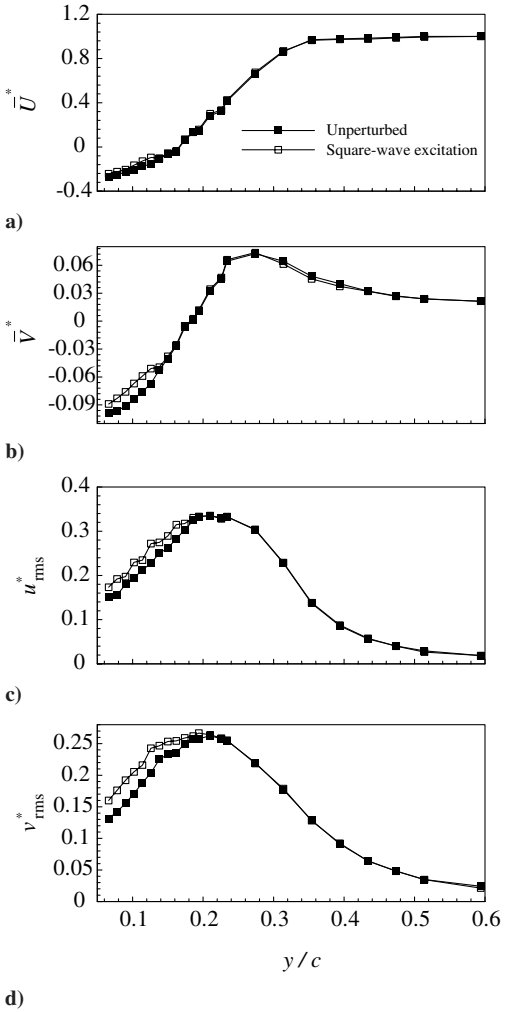

Fig. 10 Crossflow distributions of mean flow velocities and root mean square value of fluctuating flow velocities in the x and y directions at $x/c = 0.248$ with and without perturbation: a) $\bar{U}^*$, b) $\bar{V}^*$, c) u^*_{rms}, d) v^*_{rms}. $\alpha = 14$ deg.

large-scale vortex would have the ability to entrain the high-momentum incoherent fluid into its core, enhancing the coalescence or mergence of small vortices. The more concentrated vortex would carry more favorable circulation with a lower pressure above the airfoil surface, thus producing a higher lift force than the uncontrolled case. Based on similar physics, Unal and Rockwell [33] and Zhang et al. [34] also found the formation of large-scale vortices in the wake of a cylinder, which was responsible for the lift enhancement. Meanwhile, the concentrated vortex would transfer high-momentum fluid from the freestream into the boundary layer around the airfoil surface, contributing to the larger magnitudes of $\bar{U}^*$ and $\bar{V}^*$, and consequently postpone flow separation from the airfoil.

The present experimental data corroborate the analysis of Wu et al. [24]. The measured f_s (the hot wire was placed at $x/c = 0.008$ and $y/c = 0.15$) for $12 \le \alpha \le 20$ deg was locked into $f_p = 8$ Hz, especially when the square-wave excitation was introduced, as evident in Fig. 13. This might be due to the fact that the unperturbed f_s was measured at about 8 Hz within this α range, which could also be approximately estimated using the equation $f_s = U_\infty Sr/[c\sin(\alpha)]$ [35]. Here Sr stands for the corresponding Strouhal number at each α. Furthermore, the natural frequency f_n of the actuators was presently designed to be 8 Hz, under which $Y_{p,\text{rms}}$ reached the maximum, up to 1.8 mm (Fig. 2). The large $Y_{p,\text{rms}}$ might further strengthen the flow to be locked into the perturbation, which had been observed by Zhang et al. [15]. The strong lock-in phenomenon led to the formation of the large-scale vortices and, subsequently, the enhancement in the vortex circulation above the airfoil (see the examples in Figs. 11c and 12c). In the meantime, the momentum in the boundary layer above the airfoil surface was increased under control (see examples in Figs. 8–10). Therefore, the present lift force on the airfoil and the flow separation from the airfoil for $12 \le \alpha \le 20$ deg, according to Wu et al. [24], would be subjected to effective enhancement and impairment, respectively. The impaired flow separation would further lead to an increase in lift force and a decrease in drag force as well, consistent with the results in Fig. 5 and Table 1. Note the unperturbed and perturbed f_s at $\alpha = 14$ deg were almost equal to each other (Fig. 13), implying the occurrence of a rather strong resonant phenomenon in the flow. To confirm this, the control effect on the u spectrum E_u at three different streamwise locations above the airfoil, i.e., $x/c = 0.008$, 0.128, and 0.248 ($y/c = 0.15$), where the control effect on flow separation is evident (Figs. 8–11), was examined based on LDA measurements, shown in Fig. 14. Without perturbation, a very small peak in E_u, due to vortex shedding from the airfoil, occurs at $f_s = 8$ Hz or $f^*_s = 0.67$. The nearby number indicates its peak magnitude. The asterisk denotes the normalization of frequency f by c and U_∞, i.e., $f^* = fc/U_\infty$. With the perturbation applied ($f^*_p = f^*_s$), the peak magnitude at f^*_s was greatly enlarged, irrespective of locations, suggesting the significant amplification in the energy of the dominant vortices as a result of the synchronization between f^*_p and f^*_s. Similar measurements to those shown in Fig. 14 were also conducted at other α within the effective α range (not shown), but the modification in E_u at f^*_s was less obvious. Subsequently, the best control performance at

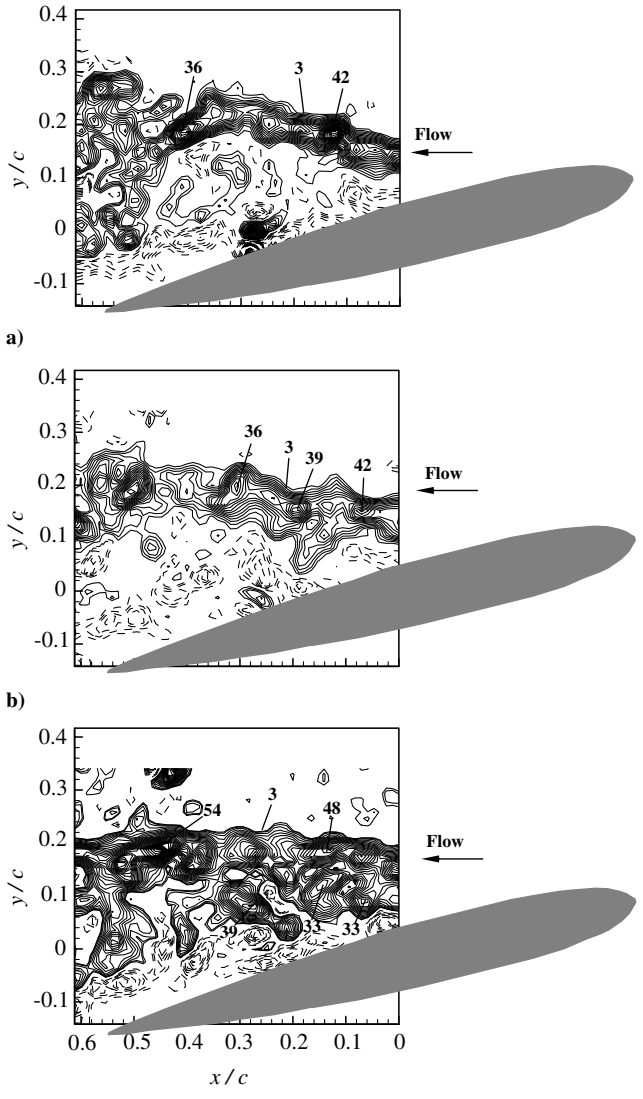

Fig. 11 Typical PIV-measured isocontours of spanwise vorticity $\omega_z^* = \omega_z c/U_\infty$ with and without perturbation: a) unperturbed case, b) sine-wave excitation, c) square-wave excitation. $\alpha = 14$ deg. The contour increment $\Delta\omega_z^*$ is three; the cutoff level $|\omega_{zc}^*|$ is three. Flow is right to left.

$\alpha = 14$ deg may be attributed to the strongest lock-in relation between flow and perturbation.

VI. Conclusions

Control of airfoil aerodynamics at poststall attack angles has been experimentally investigated using a surface perturbation technique, which is characterized by lightweight and small-size actuators, low-energy input, and high-power efficiency. The control action was implemented through the local surface perturbation on the airfoil generated by piezoceramic actuators. The investigation leads to following conclusions:

1) The proposed perturbation technique is effective to improve airfoil aerodynamics for $12 \le \alpha \le 20$ deg. The best control performance was obtained at $\alpha = 14°$ when the square-wave excitation was used, resulting in a maximum enhancement of 35, 64, and 44% in $\bar{C}_L$, L/D, and F.M., respectively, and a maximum impairment of 23% in $\bar{C}_D$. The stall angle was increased from 11 to 14 deg. The control under square-wave excitation overwhelms that under sine-wave excitation. The difference was ascribed to the fact that a square wave consists of harmonic components as well as the perturbation frequency, which could optimally capitalize the inherent instabilities of the flow and meanwhile supply more effective excitation energy than a sine wave.

2) The control physics lie in the generation of the large-scale vortices above the airfoil. In successful control, the unstable flow separation or vortex shedding from the airfoil is locked in by the controlled surface perturbation. The lock-in phenomenon greatly enhances the main vortex strength, forming the large vortex structures above the airfoil. These large-scale vortices may increase the lift force on the airfoil and the momentum in the airfoil boundary layer. The latter may act to suppress flow separation. Subsequently,

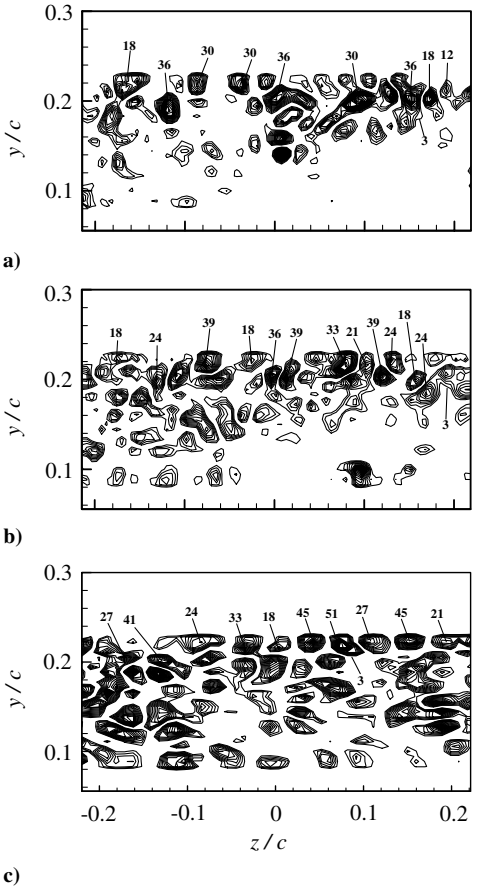

Fig. 12 Typical PIV-measured isocontours of streamwise vorticity $\omega_x^* = \omega_x c/U_\infty$ with and without perturbation ($x/c = 0.008$): a) unperturbed case, b) sine-wave excitation, c) square-wave excitation. $\alpha = 14$ deg. The contour increment $\Delta\omega_x^*$ is three; the cutoff level $|\omega_{xc}^*|$ is three.

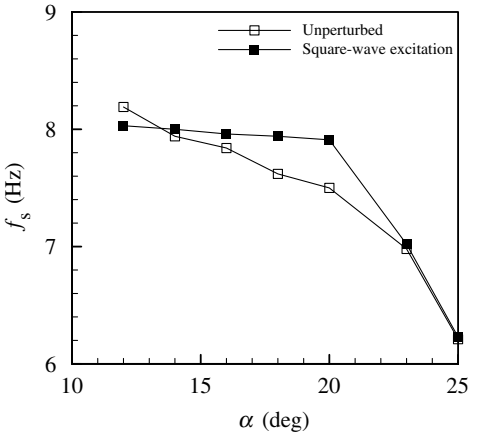

Fig. 13 Vortex shedding frequency f_s at different attack angles α with and without perturbation. The square-wave excitation was used.

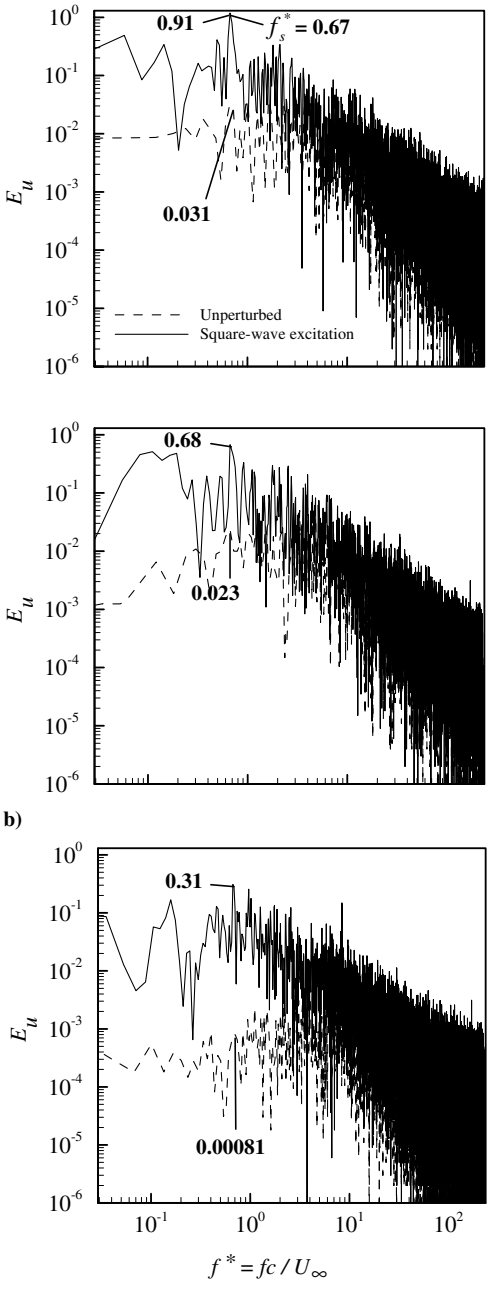

Fig. 14 Control effect on the variation of u spectrum, i.e., E_u, with different streamwise locations ($y/c = 0.15$): a) $x/c = 0.008$, b) $x/c = 0.128$, c) $x/c = 0.248$. The square-wave excitation was used. $\alpha = 14$ deg.

the final lift and drag forces on the airfoil would be increased and decreased, respectively.

Acknowledgments

The authors wish to acknowledge support from Research Grants Council of Hong Kong Special Administrative Region (Project Nos. PolyU 5132/07E and PolyU 5334/06E). The third author also wishes to acknowledge the support from a special fund for recently promoted Chair Professors given by Hong Kong Polytechnic University.

References

[1] Anderson, J. D., Jr., *Introduction to Flight*, McGraw–Hill, New York, 2005.

[2] Schlichting, H., *Boundary Layer Theory*, McGraw–Hill, New York, 1979.

[3] Gad-el-Hak, M., and Bushnell, D. M., "Separation Control: Review," *Journal of Fluids Engineering*, Vol. 113, No. 1, 1991, pp. 5–30.

[4] Greenblatt, D., and Wygnanski, I. J., "Control of Flow Separation by Periodic Excitation," *Progress in Aerospace Sciences*, Vol. 36, No. 7, 2000, pp. 487–545. doi:10.1016/S0376-0421(00)00008-7

[5] Corke, T., *Design of Aircraft*, Prentice–Hall, New York, 2002.

[6] Modi, V. J., Hill, S. S., and Yokomizo, T., "Drag Reduction of Trucks Through Boundary-Layer Control," *Journal of Wind Engineering and Industrial Aerodynamics*, Vol. 54, No. 3, 1995, pp. 583–594. doi:10.1016/0167-6105(94)00074-N

[7] Seifert, A., Darabi, A., and Wygnanski, I., "Delay of Airfoil Stall by Periodic Excitation," *Journal of Aircraft*, Vol. 33, No. 4, 1996, pp. 691–698.

[8] Seifert, A., Bachar, T., Koss, D., Shepshelovich, M., and Wygnanski, I., "Oscillatory Blowing: A Tool to Delay Boundary-Layer Separation," *AIAA Journal*, Vol. 31, No. 11, 1993, pp. 2052–2060.

[9] Sinha, S. K., "Flow Separation Control with Microflexural Wall Vibrations," *Journal of Aircraft*, Vol. 38, No. 3, 2001, pp. 496–503.

[10] Zaman, K. B. M. Q., Bar-Sever, A., and Mangalam, S. M., "Effect of Acoustic Excitation on the Flow over a Low-*Re* Airfoil," *Journal of Fluid Mechanics*, Vol. 182, No. 1, 1987, pp. 127–148. doi:10.1017/S0022112087002271

[11] Hsiao, F. B., Liu, C. F., and Shyu, J. Y., "Control of Wall-Separated Flow by Internal Acoustic Excitation," *AIAA Journal*, Vol. 28, No. 8, 1990, pp. 1440–1446.

[12] Seifert, A., Eliahu, S., Greenblatt, D., and Wygnanski, I., "Use of Piezoelectric Actuators for Airfoil Separation Control," *AIAA Journal*, Vol. 36, No. 8, 1998, pp. 1535–1537.

[13] Melton, L. P., Schaeffler, N. W., Yao, C. S., and Seifert, A., "Active Control of Flow Separation from Supercritical Airfoil Leading-Edge Flap Shoulder," *Journal of Aircraft*, Vol. 42, No. 5, 2005, pp. 1142–1149. doi:10.2514/1.10294

[14] Cheng, L., Zhou, Y., and Zhang, M. M., "Perturbed Interaction Between Vortex Shedding and Induced Vibration," *Journal of Fluids and Structures*, Vol. 17, No. 7, 2003, pp. 887–901. doi:10.1016/S0889-9746(03)00042-2

[15] Zhang, M. M., Cheng, L., and Zhou, Y., "Closed-Loop-Controlled Vortex Shedding from a Flexibly Supported Square Cylinder Under Different Schemes," *Physics of Fluids*, Vol. 16, April 2004, pp. 1439–1448. doi:10.1063/1.1687413

[16] Zhang, M. M., Cheng, L., and Zhou, Y., "Closed-loop controlled vortex-airfoil interactions," *Physics of Fluids*, Vol. 18, April 2006, p. 046102. doi:10.1063/1.2189287

[17] Huang, J. F., Zhou, Y., and Zhou, T. M., "Three-Dimensional Wake Structure Measurement Using a Modified PIV Technique," *Experiments in Fluids*, Vol. 40, No. 6, 2006, pp. 884–896. doi:10.1007/s00348-006-0126-9

[18] Hoarau, Y., Braza, M., Ventikos, Y., Faghani, D., and Tzabiras, G., "Organized Modes and the Three-Dimensional Transition to Turbulence in the Incompressible Flow Around a NACA0012 Wing," *Journal of Fluid Mechanics*, Vol. 496, Dec. 2003, pp. 63–72. doi:10.1017/S0022112003006530

[19] Copeland, B. M., Buckley, J. D., Bryant, R. G., Fox, R. L., and Hellbaum, R. F., "THUNDER: An Ultra-High Displacement Piezoelectric Actuator," NASA Langley Research Center, VA 23681-0001, 1999.

[20] Wise, S. A., "Displacement Properties of RAINBOW and THUNDER Piezoelectric Actuators," *Sensors and Actuators A (Physical)*, Vol. 69, No. 1, 1998, pp. 33–38. doi:10.1016/S0924-4247(97)01745-7

[21] Zhang, M. M., Zhou, Y., and Cheng, L., "Spring-Supported Cylinder Wake Control," *AIAA Journal*, Vol. 41, No. 8, 2003, pp. 1500–1506.

[22] Maskell, E. C., "Theory of the Blockage Effects on Bluff Bodies and Stalled Wings in a Closed Wind Tunnel," Aeronautical Research Council Repts. and Memo., No. 3400, Nov. 1963.

[23] Michos, A., Bergeles, G., and Athanassiadis, N., "Aerodynamic Characteristics of NACA0012 Airfoil in Relation to Wind Generators," *Wind Engineering*, Vol. 7, No. 4, 1983, pp. 247–262.

[24] Wu, J. Z., Lu, X. Y., Denny, A. G., Fan, M., and Wu, J. M., "Post-Stall Flow Control on an Airfoil by Local Unsteady Forcing," *Journal of Fluid Mechanics*, Vol. 371, April 1998, pp. 21–58. doi:10.1017/S0022112098002055

[25] Margalit, S., Greenblatt, D., Seifert, A., and Wygnanski, I., "Delta Wing

Stall and Roll Control Using Segmented Piezoelectric Fluidic Actuators," *Journal of Aircraft*, Vol. 42, No. 3, 2005, pp. 698–709. doi:10.2514/1.6904

[26] Amitay, M., Smith, D. R., Kibens, V., Parekh, D. E., and Glezer, A., "Aerodynamic Flow Control over an Unconventional Airfoil Using Synthetic Jet Actuators," *AIAA Journal*, Vol. 39, No. 3, 2001, pp. 361–370.

[27] Bons, J. P., Sondergaard, R., and Rivir, R. B., "Fluid Dynamics of LPT Blade Separation Control Using Pulsed Jets," *Journal of Turbomachinery*, Vol. 124, No. 1, 2002, pp. 77–85. doi:10.1115/1.1425392

[28] Dandois, J., Garnier, E., and Sagaut, P., "Numerical Simulation of Active Separation Control by a Synthetic Jet," *Journal of Fluid Mechanics*, Vol. 574, Feb. 2007, pp. 25–58. doi:10.1017/S0022112006003995

[29] Amitay, M., and Giezer, A., "Role of Actuation Frequency in Controlled Flow Reattachment over Stalled Airfoil," *AIAA Journal*, Vol. 40, No. 2, 2002, pp. 203–216.

[30] Glezer, A., Amitay, M., and Honohan, A. M., "Aspects of Low- and High-Frequency Aerodynamics Flow Control," *AIAA Journal*, Vol. 43, No. 7, 2005, pp. 1501–1511. doi:10.2514/1.7411

[31] Bar-Sever, A., "Separation Control on an Airfoil by Periodic Forcing," *AIAA Journal*, Vol. 27, No. 6, 1989, pp. 820–821.

[32] Cantwell, B. J., and Coles, D., "Experimental Study of Entrainment and Transport in the Turbulent Near Wake of a Circular Cylinder," *Journal of Fluid Mechanics*, Vol. 136, April 1983, pp. 321–374. doi:10.1017/S0022112083002189

[33] Unal, M. F., and Rockwell, D., "On the Vortex Formation from a Cylinder, Part 1: The Initial Instability," *Journal of Fluid Mechanics*, Vol. 190, April 1988, pp. 491–512. doi:10.1017/S0022112088001429

[34] Zhang, M. M., Zhou, Y., and Cheng, L., "Closed-Loop-Manipulated Wake of a Stationary Square Cylinder," *Experiments in Fluids*, Vol. 39, No. 1, 2005, pp. 75–85. doi:10.1007/s00348-005-0979-3

[35] Katz, J., "Discrete Vortex Method for the Non-Steady Separated Flow over an Airfoil," *Journal of Fluid Mechanics*, Vol. 102, April 1981, pp. 315–328. doi:10.1017/S0022112081002668

F. Coton
Associate Editor